

1 **Measurement report: Diurnal variations of brown carbon during two distinct seasons in a**  
2 **megacity in Northeast China**

3 Yuan Cheng<sup>1</sup>, Xu-bing Cao<sup>1</sup>, Jiu-meng Liu<sup>1,\*</sup>, Ying-jie Zhong<sup>1</sup>, Qin-qin Yu<sup>1</sup>, Qiang Zhang<sup>2</sup> and Ke-  
4 bin He<sup>3</sup>

5 <sup>1</sup> State Key Laboratory of Urban Water Resource and Environment, School of Environment, Harbin  
6 Institute of Technology, Harbin 150090, China

7 <sup>2</sup> Ministry of Education Key Laboratory for Earth System Modeling, Department of Earth System  
8 Science, Tsinghua University, Beijing 100084, China

9 <sup>3</sup> State Key Joint Laboratory of Environment Simulation and Pollution Control, School of  
10 Environment, Tsinghua University, Beijing 100084, China

11 \*Corresponding author. Jiu-meng Liu (jiumengliu@hit.edu.cn).

12 **Abstract**

13 Brown carbon (BrC) represents an important target for the “win-win” strategy of mitigating climate  
14 change and improving air quality. However, estimating co-benefits of BrC control remains difficult  
15 for China, partially because current measurement results are insufficient to represent the highly  
16 variable emission sources and meteorological conditions across different regions. In this study, we  
17 investigated, for the first time, the diurnal variations of BrC during two distinct seasons in a  
18 megacity in Northeast China. The winter campaign conducted in January of 2021 was characterized  
19 by low temperatures rarely seen in other Chinese megacities (down to about  $-20\text{ }^{\circ}\text{C}$ ). The mass  
20 absorption efficiencies of BrC at 365 nm ( $\text{MAE}_{365}$ ) were found to be  $\sim 10\%$  higher at night. The  
21 variations of  $\text{MAE}_{365}$  could not be explained by the influence of residential biomass burning  
22 emissions or secondary aerosol formation, but were strongly associated with the changes of a  
23 diagnostic ratio for the relative importance of coal combustion and vehicle emissions ( $R_{S/N}$ ). Given  
24 that most coal combustion activities were uninterrupted, the higher nighttime  $\text{MAE}_{365}$  in winter  
25 were attributed primarily to increased emissions from heavy-duty diesel trucks. The spring

26 campaign conducted in April of 2021 was characterized by frequent occurrences of agricultural fires,  
27 as supported by the intensive fire hotspots detected around Harbin and the more-than-doubled  
28 levoglucosan to organic carbon ratios (LG/OC) compared to winter campaign. In spring, MAE<sub>365</sub>  
29 depended little on  $R_{S/N}$  but exhibited a strong positive correlation with LG/OC, suggesting open  
30 burning emissions as the dominant influencing factor for BrC's light absorption capacity. MAE<sub>365</sub>  
31 were ~70% higher at night for the spring campaign, pointing to the prevalence of nighttime  
32 agricultural fires, which were presumably in response to local bans on open burning. It is noteworthy  
33 that the agricultural fire emissions resulted in distinct peak at ~365 nm for the light absorption  
34 spectra of BrC, and candidates for the compounds at play were inferred to be aromatic species with  
35 nitro-functional groups. The presence of the ~365 nm peak complicated the determination of  
36 absorption Ångström exponents for the agricultural fire-impacted samples. In addition, the ~365 nm  
37 peak became much less significant during the day, likely due to photo-bleaching of the relevant  
38 chromophores.

## 39 **1. Introduction**

40 Light-absorbing organic carbon, i.e., brown carbon (BrC), exerts important yet poorly  
41 understood effects on climate and the environment (Brown et al., 2018; Zeng et al., 2020; Sand et  
42 al., 2021). As a mixture of numerous organic compounds from both primary emissions and  
43 secondary formation, BrC exhibits extreme complexity in spectroscopy, composition and evolution  
44 (Laskin et al., 2015; Brege et al., 2021; Washenfelder et al., 2022). Measurement techniques for BrC  
45 absorption mainly fell into two categories, including solvent extraction followed by light absorption  
46 spectrum measurement (Chen and Bond, 2010; Hecobian et al., 2010) and apportionment of total  
47 aerosol absorption to the contributions from black carbon and BrC (Yang et al., 2009; Lack et al.,  
48 2012). So far, consistency between BrC results from these two types of approaches has not been  
49 addressed, with variable relationships, either linear or non-linear, and unclear influencing factors  
50 (Kumar et al., 2018; Zeng et al., 2022). This inconsistency introduced substantial difficulties to the  
51 integration of BrC measurement results across studies and regions (Wang et al., 2022), which is  
52 essential for unfolding the links between BrC sources and optical properties. In addition, efforts  
53 were also made to explain BrC absorption on a molecular level. Several techniques were shown to  
54 be powerful, such as electrospray ionization Fourier transform ion cyclotron resonance mass  
55 spectrometry (ESI FT-ICR MS; Wozniak et al., 2008; Jiang et al., 2021; Zeng et al., 2021), high  
56 performance liquid chromatography coupled with high resolution mass spectrometry  
57 (HPLC/HRMS; Lin et al., 2018; Huang et al., 2022; Xu et al., 2022), and two-dimensional gas  
58 chromatography with time of flight mass spectrometer (GC×GC-ToF-MS; Huo et al., 2021). These  
59 techniques were more frequently applied to laboratory-generated primary or secondary BrC (e.g.,  
60 Lin et al., 2015), which usually had less complex composition than ambient BrC and thus showed

61 relatively high fraction of resolvable chromophores, e.g., up to ~85% for those emitted by biomass  
62 burning (Huang et al., 2022).

63 The absorbing nature of BrC makes it a non-negligible contributor to positive radiative forcing  
64 (Saleh, 2020), while the considerable contribution of organic aerosol to fine particulate matter  
65 (PM<sub>2.5</sub>) makes BrC an important source of air pollution (Wang et al., 2019). Consequently, BrC  
66 represents a key species for the “win-win” strategy of mitigating climate change and improving air  
67 quality. Given the highly variable emission sources and meteorological conditions across different  
68 regions in China, field observational results on BrC are far from being enough to constrain air  
69 quality and climate models, limiting the ability to evaluate the co-benefits of BrC control. In this  
70 study, we focused on a largely unexplored city cluster, the Harbin-Changchun (HC) metropolitan  
71 area in Northeast China. Compared to other regions with intensive studies of BrC as well as other  
72 air pollutants (e.g., the North China Plain), HC was characterized by extremely cold winter and  
73 strong impacts of biomass burning on top of other anthropogenic emissions (e.g., from coal  
74 combustion). The first feature was related to the relatively high latitudes of HC. For example, as the  
75 northernmost megacity in China, Harbin has an average temperature of about -20°C in January,  
76 significantly lower than that of Beijing (~0 °C). The second feature was related to the massive  
77 agricultural sector in HC. Until recently, open burning was still an irreplaceable approach for the  
78 disposal of crop residues in this region, presumably because the amount of agricultural wastes was  
79 too huge for the capacity of sustainable use. The agricultural fires frequently resulted in heavily-  
80 polluted episodes with high PM<sub>2.5</sub> concentrations rarely encountered in other Chinese megacities  
81 (e.g., hourly-average of ~1000 µg/m<sup>3</sup> in Harbin; Li et al., 2019). These two features highlighted the  
82 uniqueness of HC for haze studies in China.

83 This measurement report, for the first time, presented field observational results on the diurnal  
84 variations of BrC during two distinct seasons, i.e., a frigid winter and an agricultural fire-impacted  
85 spring, in the central city of HC. Drivers for the diurnal variations were discussed based on  
86 indicators of various sources. Particularly, the agricultural fires were found to result in unique  
87 absorption spectra of brown carbon. This study provided implications for parameterization of BrC  
88 in climate models.

## 89 **2. Methods**

### 90 **2.1 Field sampling**

91 Daytime and nighttime PM<sub>2.5</sub> samples were collected on the campus of Harbin Institute of  
92 Technology (HIT) during winter and spring of 2021. HIT was surrounded by residential and  
93 commercial areas, without major industrial sources nearby, and thus represented a typical urban site.  
94 The sampling was done by a mass flow controlled high-volume sampler (TE-6070BLX-2.5-HVS;  
95 Tisch Environmental, Inc., OH, USA), which was operated at a flow rate of 1.13 m<sup>3</sup>/min using pre-  
96 baked quartz-fiber filters (8" × 10", 2500 QAT-UP; Pall Corporation, NY, USA). To avoid rush hours  
97 and considering the relatively early sunset time in winter (~16:00–17:00), daytime and nighttime  
98 samples were collected from 9:00 to 16:00 and from 21:00 to 5:00 of the next day, respectively. The  
99 winter campaign covered the entire January of 2021, and the spring campaign was conducted during  
100 10–30 April, 2021.

### 101 **2.2 Laboratory analysis**

102 Two punches with diameters of 20 mm were taken from each sample, combined and then  
103 extracted by deionized water. The water extract was analyzed using a Dionex ion chromatography  
104 system (ICS-5000<sup>+</sup>; Thermo Fisher Scientific Inc., MA, USA). Levoglucosan, an organic tracer for

105 biomass burning, was determined by the high-performance anion-exchange chromatography  
106 coupled to pulsed amperometric detection (HPAEC-PAD) method (Engling et al., 2006; Yttri et al.,  
107 2015). Inorganic ions such as nitrate, sulfate, chloride, ammonium and potassium were also  
108 measured. Linear regression of the total cation concentration on that of total anion (both in  $\mu\text{eq}/\text{m}^3$ )  
109 led to a slope of  $1.14 \pm 0.01$  (intercept was set as zero;  $r = 0.99$ ), indicating a neutralized feature of  
110 the Harbin aerosols.

111 Two punches with diameters of 47 mm were taken from each sample and used to determine  
112 carbon fractions. Following the method developed by Chen and Bond (2010) and refined by Cheng  
113 et al. (2016), one punch was directly measured for organic carbon and elemental carbon, while the  
114 other punch was immersed in methanol (HPLC grade; Fisher Scientific Company L.L.C., NJ, USA)  
115 for an hour without stirring or sonication, dried in air for another hour, and then analyzed. Both  
116 punches were measured by a Thermal/Optical Carbon Analyzer (DRI-2001; Atmoslytic Inc., CA,  
117 USA), which was operated with two commonly-used temperature protocols (i.e., IMPROVE-A and  
118 NIOSH) and transmittance charring correction. The difference of total carbon (TC) concentrations  
119 between the untreated and extracted punches ( $\text{TC}_{\text{untreated}} - \text{TC}_{\text{extracted}}$ ) was used to represent the  
120 amount of organic carbon that is soluble in methanol (MSOC). Given that the TC measurement was  
121 independent of the temperature protocol used, both  $\text{TC}_{\text{untreated}}$  and  $\text{TC}_{\text{extracted}}$  were determined as the  
122 averages of total carbon results from IMPROVE-A and NIOSH. A benefit of this approach was that  
123 the uncertainty of MSOC ( $\sigma$ ) could be estimated for each sample based on the parallel TC  
124 measurements by different protocols:

$$125 \quad \sigma = \sqrt{(\text{SD of } \text{TC}_{\text{untreated}})^2 + (\text{SD of } \text{TC}_{\text{extracted}})^2} / (\text{TC}_{\text{untreated}} - \text{TC}_{\text{extracted}})$$

126 where SD indicates standard deviation. In this study,  $\sigma$  averaged  $3.3 \pm 2.9\%$  with a median of 2.4%.

127 In addition, organic compounds that are in-soluble in methanol, i.e., MIOC, was measured as the  
128 organic carbon concentration of the extracted punch. Unless stated otherwise, (i) OC involved in  
129 the following discussions indicates the sum of MSOC and MIOC, and correspondingly, EC indicates  
130 elemental carbon measured by the extracted punch; and (ii) all the carbonaceous aerosol  
131 concentrations are based on IMPROVE-A, except MSOC which did not rely on analytical protocol.  
132 The MSOC to OC ratios averaged  $0.90 \pm 0.05$ , indicating an overall high extraction efficiency of  
133 methanol for dissolving organic aerosols.

134 Light absorption spectra of the methanol extracts were measured over the wavelength ( $\lambda$ ) range  
135 of 200–1110 nm, using a spectrophotometer coupled with a 2.5-m long liquid waveguide capillary  
136 cell (LWCC; World Precision Instrument, FL, USA). The spectrophotometer, consisting of a DH-  
137 mini UV-VIS-NIR light source and a Maya2000 Pro spectrometer (Ocean Optics Inc., FL, USA),  
138 provided wavelength-resolved optical attenuation ( $ATN_\lambda$ ) of the dissolved BrC, which could then  
139 be converted to BrC absorption coefficient [ $(b_{\text{abs}})_\lambda$ ] (Hecobian et al., 2010). The ratio of  $(b_{\text{abs}})_\lambda$  to  
140 MSOC concentration was considered the bulk mass absorption efficiency ( $MAE_\lambda$ ) of brown carbon,  
141 given the close-to-one MSOC/OC. The wavelength dependence of BrC absorption was determined  
142 based on  $\ln(ATN_\lambda)$  and  $\ln(\lambda)$ , and was expressed as the absorption Ångström exponent (AAE). The  
143 AAE calculation was performed over 310–460 nm, the same  $\lambda$  range adopted by previous studies  
144 conducted at the same site using the same laboratory analysis procedures (Cheng et al., 2022a).

### 145 **2.3 Additional data sets used**

146 Air quality data and meteorological data were obtained with a time resolution of 1 hour from  
147 the China National Environmental Monitoring Center (CNEMC; <https://air.cnemc.cn:18007/>, last  
148 access: 1 January, 2023) and Weather Underground (<https://www.wunderground.com/>, last access:

149 1 January, 2023), respectively. CNEMC operated 12 monitoring sites in Harbin, with 3 of them  
150 located within ~5 km from the HIT sampling site. The reconstructed PM<sub>2.5</sub> masses, which were  
151 derived from observational results on aerosol compositions at HIT, were generally in line with the  
152 fine particle concentrations directly measured at the nearby CNEMC sites. Here the reconstructed  
153 PM<sub>2.5</sub> was calculated as the sum of organic matter ( $1.6 \times \text{OC}$ ), elemental carbon and inorganic ions.  
154 Comparison of the reconstructed and directly-measured PM<sub>2.5</sub> concentrations showed relative  
155 standard deviations of 9–11% (in terms of median value) for the three CNEMC sites nearby,  
156 demonstrating HIT as a representative urban site for Harbin. In this study, only the air quality data  
157 from the nearest CNEMC site, i.e., Taiping Hongwei Park, were further investigated together with  
158 the aerosol components measured at HIT.

### 159 **3. Results and discussion**

#### 160 **3.1 Why was the wintertime brown carbon more absorbing at night?**

161 The wavelength-resolved  $b_{\text{abs}}$  and MAE were primarily explored at 365 nm, and the  
162 corresponding values were referred to as  $(b_{\text{abs}})_{365}$  and MAE<sub>365</sub>, respectively.  $(b_{\text{abs}})_{365}$  and MSOC  
163 correlated strongly for the winter campaign (Figure 1a), that the linear regression of  $(b_{\text{abs}})_{365}$  against  
164 MSOC led to an  $r$  value of 0.97 and a slope of  $1.63 \pm 0.02 \text{ m}^2/\text{gC}$  (with the intercept set as zero;  
165 MAE<sub>365</sub> averaged  $1.55 \pm 0.18 \text{ m}^2/\text{gC}$ ). However, as shown in Figure 1b, the nighttime samples were  
166 found to exhibit higher MAE<sub>365</sub> values (averaging  $1.61 \pm 0.15 \text{ m}^2/\text{gC}$ ) than the daytime ones  
167 (averaging  $1.48 \pm 0.18 \text{ m}^2/\text{gC}$ ), with significant differences at the 95% confidence level (2-tailed  $p$   
168 = 0.004). In this study, we did not perform source apportionment analysis for brown carbon due to  
169 the relatively small number of samples collected. Instead, several indirect indicators were  
170 introduced to interpret the diurnal variations of MAE<sub>365</sub>. Statistical results for the comparisons



171 performed in the following discussions are summarized in Table S1.

172 The first indicator was the levoglucosan to OC ratio (LG/OC; on a basis of carbon mass, the  
173 same hereinafter). In general, higher LG/OC values indicate a stronger contribution of biomass  
174 burning (BB) emissions to OC. The BB activities in January could be attributed primarily to  
175 household use of biofuels, e.g., for heating and cooking. This is because (i) few fire hotspot was  
176 detected in Harbin and surrounding regions throughout the winter campaign (Figure 2a), and (ii) the  
177 relationship between LG and water-soluble potassium ( $K^+$ ), another commonly-used BB tracer, did  
178 not show evidence for apparent influence of open burning (Figure 3a). As suggested by previous  
179 studies conducted during heating season in Harbin (Cheng et al., 2022b), the LG to  $K^+$  ratios were  
180 relatively low and constant (~0.5) with the absence of agricultural fires, but became substantially  
181 higher (typically above 1.0) during open burning episodes. This pattern was attributed to the  
182 relatively low combustion efficiencies (CE) of agricultural fires, which favored the increase of LG  
183 emissions but would not change  $K^+$  emissions significantly (Gao et al., 2003). It should be noted  
184 that in Cheng et al. (2022b), CE were not directly measured for different types of burning activities  
185 and instead were investigated based on the ratios of BB organic carbon to BB elemental carbon ( $R_{BB}$ ,  
186 derived from positive matrix factorization, i.e., PMF, analysis). Substantial increases of  $R_{BB}$  were  
187 repeatedly observed during open burning episodes occurring in different seasons, e.g., winter or  
188 spring depending on the regulatory policies. Thus the agricultural fires were inferred to have  
189 relatively low CE levels compared to residential burning of crop residues (Cheng et al., 2022b), as  
190 BB source emission studies typically showed a decreasing trend for the emission ratio of organic  
191 carbon to elemental carbon with increasing combustion efficiency (Pokhrel et al., 2016; McClure et  
192 al., 2020). Actually, crop residues burned on farmland were usually not intentionally dried and thus

193 could have relatively high water contents. This may partially explain the relatively low CE of  
194 agricultural fires. In the present study, LG correlated strongly with  $K^+$  for the entire January ( $r =$   
195  $0.96$ , with a slope, i.e.,  $\Delta LG/\Delta K^+$ , of  $0.55 \pm 0.02$ ; Figure 3a) and the LG to  $K^+$  ratios averaged  $0.46$   
196  $\pm 0.11$ , pointing to the dominance of residential burning in BB emissions. In addition, the residential  
197 burning activities were more intensive at night, as can be seen from the elevated LG/OC compared  
198 to daytime results ( $1.10 \pm 0.26\%$  vs.  $0.88 \pm 0.22\%$ , 2-tailed  $p = 0.001$ ; Figure 1c). Comparison of  
199 the LG to EC ratios between the nighttime and daytime samples ( $0.22 \pm 0.06$  vs.  $0.15 \pm 0.05$ , 2-  
200 tailed  $p = 0.000$ ) reached the same conclusion. Indeed, biomass burning could emit a number of  
201 strong chromophores such as nitrogen-containing aromatic compounds (Mohr et al., 2013; Lin et  
202 al., 2016, 2017; Xie et al., 2019; Salvador et al., 2021). However, for the January samples,  $MAE_{365}$   
203 did not show clear dependence on LG/OC or LG/EC ( $r = 0.42$  and  $0.12$ , respectively; Figure 1e),  
204 suggesting that in addition to BB emissions, there must exist other factors that were more  
205 responsible for the diurnal variations of wintertime  $MAE_{365}$ .

206 The second indicator was  $R_{S/N}$ , defined as the ratio of (n-sulfur dioxide + n-sulfate) to (n-  
207 nitrogen dioxide + n-nitrate), where “n” indicates molar concentration. Given that sulfate and nitrate  
208 are typically considered as secondary,  $R_{S/N}$  could be roughly traced back to the emission ratios of  
209 sulfur dioxide ( $SO_2$ ) to nitrogen oxides ( $NO_x$ ), i.e.,  $E_{S/N}$ , from combustion of various types of fuels  
210 (e.g., coal, gasoline, diesel and biomass). Previous studies suggested that  $E_{S/N}$  differed substantially  
211 between emissions from vehicles, coal combustion and biomass burning. In China, the fuel quality  
212 standards have been greatly strengthened for on-road vehicles since early 2000s, e.g., the maximum  
213 sulfur content allowed in diesel was reduced from 2000 ppm (required by the China I standard  
214 implemented in 2002) to 10 ppm (required by the China V standard implemented in 2017). Thus,

215 recent studies on vehicular exhausts typically suggested that the SO<sub>2</sub> emission factors (EF-SO<sub>2</sub>)  
216 were about two orders of magnitude lower than those of NO<sub>x</sub> (EF-NO<sub>x</sub>; Zhang et al., 2015; Li et  
217 al., 2019) and consequently, the corresponding  $E_{S/N}$  should be approximately  $\sim 10^{-2}$ . EF-SO<sub>2</sub> were  
218 also usually lower than EF-NO<sub>x</sub> for biomass burning (Zhang et al., 2000; McMeeking et al., 2009;  
219 Liu et al., 2016; Wu et al., 2022), but their differences were not as large as those observed in vehicle  
220 emissions, leading to  $E_{S/N}$  values of  $\sim 10^{-1}$ . Unlike vehicles or biomass burning, coal combustion  
221 usually resulted in higher EF-SO<sub>2</sub> compared to EF-NO<sub>x</sub> (Zhang et al., 2000; Du et al., 2017; Li et  
222 al., 2017), which could be translated to  $E_{S/N}$  values of above one. On the other hand, primary species  
223 could be transformed rapidly during atmospheric aging, e.g., a sharp loss of NO<sub>x</sub> and a  
224 corresponding burst in nitrate were observed shortly after emission when tracking plumes from  
225 diesel trucks (Shen et al., 2021) and agricultural fires (Akagi et al., 2012; Liu et al., 2016). Thus it  
226 should be acceptable to assume that for the pollutants emitted by a specific source, the  $R_{S/N}$  of aged  
227 plumes was generally comparable with the  $E_{S/N}$  of fresh emissions.

228 The ambient  $R_{S/N}$  averaged  $0.6 \pm 0.2$  during the winter campaign, differing substantially from  
229 the  $E_{S/N}$  of coal combustion or vehicle emissions but in the same order of magnitude as the  $E_{S/N}$  of  
230 biomass burning. Actually, no evidence supported BB emissions as a major regulating factor for  
231  $R_{S/N}$ , e.g., as indicated by the insignificant correlations between  $R_{S/N}$  and LG/EC ( $r = 0.24$  and  $0.01$   
232 for the daytime and nighttime samples, respectively). Then  $R_{S/N}$  was expected to be more sensitive  
233 to the changes of coal combustion and vehicle emissions, e.g., increase of coal combustion  
234 emissions would effectively elevate  $R_{S/N}$  whereas higher vehicle emissions favor the decrease of  
235  $R_{S/N}$ . During the winter campaign, lower  $R_{S/N}$  were observed at night (Figure 1d), averaging  $0.5 \pm$   
236  $0.1$  compared to an average  $R_{S/N}$  of  $0.7 \pm 0.2$  for the daytime samples (2-tailed  $p = 0.000$ ). In

237 principle, this pattern could be caused by decreased coal combustion emissions and/or increased  
238 vehicle emissions at night. However, it seemed that the former did not play an important role, since  
239 many coal combustion activities (e.g., those for heating supply, power generation and some  
240 industrial processes) were uninterrupted, i.e., would not be stopped at night (Lian et al., 2020; Chu  
241 et al., 2021; Yuan et al., 2021). Then the most likely cause for the lower nighttime  $R_{S/N}$  was increased  
242 vehicle emissions. According to the Road Traffic Regulations released by Harbin, heavy-duty diesel  
243 trucks (HDDT), which are known to include high- or super-emitters (Dallmann et al., 2012), are  
244 allowed to run on the roads in the main urban area only from 21:00 to 5:00 of the next day. This to  
245 a large extent explains the inference on the increase of vehicle emissions during nighttime.  $MAE_{365}$   
246 exhibited a clear negative dependence on  $R_{S/N}$  for all the winter samples (Figure 1f), suggesting  
247 vehicle emissions, especially those from HDDT, as a dominant influencing factor for  $MAE_{365}$  (under  
248 the precondition of relatively stable coal combustion emissions).

249 The last two indicators were associated with secondary aerosol formation, including the sulfur  
250 oxidation ratio (SOR) and the nitrogen oxidation ratio (NOR) defined as  $n\text{-sulfate}/(n\text{-sulfate} + n\text{-}$   
251  $SO_2)$  and  $n\text{-nitrate}/(n\text{-nitrate} + n\text{-}NO_2)$ , respectively. The entire winter campaign experienced low  
252 temperatures, which averaged  $-16 \pm 5$  and  $-21 \pm 6$  °C for the daytime and nighttime samples,  
253 respectively. In general, the transformation of gaseous precursors to secondary inorganic ions was  
254 inefficient in the frigid atmosphere, as indicated by the overall low levels of both SOR and NOR.  
255 However, both indicators exhibited noticeable differences between daytime and nighttime samples.  
256 The diurnal variation of SOR was found to be associated with the higher relative humidity (RH)  
257 levels at night (Figure 4a). For the vast majority of winter samples, RH fell into the ranges of 60–  
258 80 and 70–90% during daytime and nighttime, respectively. SOR were largely unchanged when RH

259 increased from 60–70% to 70–80% during the day, whereas for the common RH range shared by  
260 the daytime and nighttime samples (i.e., 70–80%), SOR tended to be slightly lower at night, likely  
261 due to the drop of temperatures. In addition, a positive dependence of SOR on RH was evident for  
262 the nighttime samples. Although SOR showed almost the same median values (~0.1) for the RH  
263 ranges of 70–80 and 80–90% at night, relatively high SOR levels of above 0.2 were more frequently  
264 observed in the latter case. Such high SOR were rarely seen during the day, indicating that RH  
265 played a more important role than temperature in sulfate formation. The enhanced sulfate formation  
266 at high RH was presumably through heterogeneous reactions (Su et al., 2020; Liu et al., 2021), since  
267 the low temperatures encountered during the winter campaign did not rule out the presence of  
268 aerosol water, e.g., liquid water was observed to remain super-cooled in clouds down to  
269 temperatures of as low as  $-40$  °C (Tabazadeh et al., 2002). Compared to SOR, different patterns of  
270 diurnal variation were observed for NOR (Figure 4b). First, the difference between daytime and  
271 nighttime NOR was more significant for the RH range of 70–80%, e.g., as indicated by the larger  
272 decrease of median NOR at night (0.06, compared to a corresponding value of 0.02 for SOR).  
273 Second, the nighttime NOR elevated substantially as RH increased from 70–80% to 80–90%, but  
274 still with lower levels compared to the daytime results. Given that relatively low temperatures favor  
275 the partitioning of semi-volatile nitrate into aerosol phase, the less efficient nitrate formation at night  
276 could not be explained by the partitioning process and instead should be primarily attributed to  
277 reduced photooxidation of  $\text{NO}_2$  (Chen et al., 2020). Based on a synthesis of the diurnal variations  
278 observed for SOR and NOR, the nighttime samples were characterized by enhanced heterogeneous  
279 chemistry, which did not require sunlight as indicated by the RH-dependent increase of SOR under  
280 dark conditions, and weakened photochemical reactions. The overall effect of these two factors on

281 secondary organic aerosol (SOA) formation was inconclusive and thus it remained difficult to  
282 robustly unfold the role of SOA in the diurnal variations of  $MAE_{365}$ . Actually, it appeared that  
283  $MAE_{365}$  was not strongly influenced by SOA during the winter campaign. For example, when RH  
284 increased from 70–80% to 80–90% at night, the  $MAE_{365}$  were nearly constant (e.g., with the same  
285 average value of  $1.6 \text{ m}^2/\text{gC}$  for the two RH ranges) despite the enhancement of heterogeneous  
286 chemistry.

### 287 **3.2 Why did the springtime $MAE_{365}$ show more significant diurnal variations?**

288 Compared to the wintertime results, the average  $MAE_{365}$  was lower in spring (1.33 vs. 1.55  
289  $\text{m}^2/\text{gC}$ ) but the corresponding standard deviation was much higher (0.62 vs.  $0.18 \text{ m}^2/\text{gC}$ ), indicating  
290 that the spring samples varied more significantly with respect to the absorption capacity of brown  
291 carbon (Figure 5a). This feature could also be seen from the more pronounced diurnal variations of  
292  $MAE_{365}$  observed in spring (Figure 5b), e.g., the nighttime  $MAE_{365}$  were on average ~70% (2-tailed  
293  $p = 0.000$ ) and 10% (2-tailed  $p = 0.004$ ) larger than the daytime values during the spring and winter  
294 measurement periods, respectively. For the winter campaign, the slightly elevated  $MAE_{365}$  at night  
295 had been primarily attributed to increased vehicle emissions, as indicated by a ~35% decrease of  
296  $R_{S/N}$ . In spring,  $R_{S/N}$  were also lower at night (2-tailed  $p = 0.000$ ), by ~40% compared to the daytime  
297 results (Figure 5d). Given that the two campaigns showed comparable discrepancies between the  
298 nighttime and daytime  $R_{S/N}$ , increase of vehicle emissions at night was presumably not the dominant  
299 driver for the much stronger diurnal variations of  $MAE_{365}$  observed in spring. Actually,  $MAE_{365}$  was  
300 almost independent of  $R_{S/N}$  for the spring samples. For example, the  $MAE_{365}$  values were found to  
301 fall into two well-separated ranges (above 2 and  $\sim 0.5\text{--}1.5 \text{ m}^2/\text{gC}$ , with the former observed only at  
302 night) for the samples with relatively low  $R_{S/N}$  levels (below 0.4), indicating that reduced  $R_{S/N}$  was

303 ineffective to explain the high MAE<sub>365</sub> events encountered in spring (Figure 5f). In addition to  
304 increased vehicle emissions at night, therefore, there must exist other factors which were more  
305 responsible for the significant diurnal variations of springtime MAE<sub>365</sub>.

306 We first evaluated the influence of secondary aerosol formation. The spring campaign  
307 experienced lower RH and substantially higher temperatures compared to winter, by ~25% and  
308 30 °C, respectively. The springtime SOR appeared to be slightly lower than the wintertime results  
309 ( $0.12 \pm 0.06$  vs.  $0.15 \pm 0.07$ ), whereas an opposite pattern was observed for NOR ( $0.16 \pm 0.08$  vs.  
310  $0.12 \pm 0.06$ ). The seasonal variations of SOR and NOR provided additional evidence for the  
311 inferences that the sulfate and nitrate formation was more strongly contributed by heterogeneous  
312 and photochemical reactions, respectively. For the spring campaign, the daytime and nighttime SOR  
313 were in general comparable (Figure S1a) and no clear evidence was observed for the prevalence of  
314 heterogeneous chemistry, presumably due to the rare occurrence of high RH conditions either during  
315 the day or at night. Unlike SOR, the daytime NOR tended to be slightly higher than the nighttime  
316 results ( $0.18 \pm 0.09$  vs.  $0.14 \pm 0.08$ ; Figure S1b), pointing to enhanced photochemistry during the  
317 day. This pattern could be partially responsible for the relatively low daytime MAE<sub>365</sub>, since  
318 secondary brown carbon was typically less light-absorbing than primary BrC (Kumar et al., 2018;  
319 Cappa et al., 2020; Ni et al., 2021). However, MAE<sub>365</sub> did not exhibit clear dependence on NOR or  
320 the nitrate to OC ratio ( $\text{NO}_3^-/\text{OC}$ ), e.g., the high MAE<sub>365</sub> events were found to be associated with  
321 moderate NOR and  $\text{NO}_3^-/\text{OC}$  levels (Figure S2). Thus for the spring campaign, photochemistry  
322 should not be the major influencing factor for MAE<sub>365</sub>, either.

323 We then investigated the role of biomass burning. Unlike the wintertime results, MAE<sub>365</sub>  
324 showed a strong positive correlation with LG/OC ( $r = 0.84$ ) in spring (Figure 5e), suggesting

325 biomass burning emissions as the dominant driver for the variations of  $MAE_{365}$ . It is noteworthy  
326 that the LG to OC ratios were substantially higher in spring than in winter (2-tailed  $p = 0.000$ ), with  
327 averages of  $3.11 \pm 1.70\%$  and  $0.99 \pm 0.26\%$ , respectively. This pattern could not be explained by  
328 seasonal variations in residential consumption of biofuels, since April experienced much higher  
329 temperatures than January (averaging 11 and  $-19$  °C, respectively). Instead, the elevated springtime  
330 LG/OC should be attributed primarily to open burning, as supported by the intensive fire hotspots  
331 detected around Harbin in April (Figure 2b). The seasonal variations of LG to  $K^+$  ratio (LG/ $K^+$ ) also  
332 suggested that the dominant burning ways were different between winter and spring. Compared to  
333 the relatively small and constant LG/ $K^+$  observed in January ( $0.46 \pm 0.11$ ), the ratios were nearly  
334 tripled in April ( $1.28 \pm 0.61$ ) with more significant sample-by-sample differences (between  $\sim 0.5$ –  
335 3.5) (Figure 3b). Recalling that the transition from flaming to smoldering combustion favored the  
336 increase of LG/ $K^+$  (Gao et al., 2003), the springtime burning should have relatively low and variable  
337 combustion efficiencies. This inference was in line with the fact that the agricultural fires were  
338 usually uncontrolled, e.g., with respect to water content of crop residues and abundance of oxygen.  
339 In all, for the spring campaign, the dominant driver for the variations of LG/OC and  $MAE_{365}$  could  
340 be further identified as open burning. Subsequently, the higher LG/OC and  $MAE_{365}$  at night (Figures  
341 5b–5c) could be attributed primarily to increased agricultural fires. The preference on nighttime  
342 burning was not surprising, since the agricultural fires were illegal, i.e., nominally prohibited by the  
343 Government of Heilongjiang Province.

344 It should be noted that the agricultural fire emissions increased LG/OC but had minimal  
345 influence on  $R_{S/N}$  (Figure S3). For example, the nighttime samples collected in spring differed  
346 substantially with respect to the impact of agricultural fires, as indicated by their variable LG/OC



347 which spanned nearly one order of magnitude. However, no clear pattern was observed for  $R_{S/N}$  with  
348 increasing LG/OC, e.g., linear regression of  $R_{S/N}$  on LG/OC showed an extremely low  $r$  value of  
349 0.07.

350 The frequent occurrences of agricultural fires during April, 2021 to some extent masked the  
351 “background”  $MAE_{365}$ , i.e., the value representative for the spring conditions without significant  
352 influence of open burning. In spring, all the samples with LG/ $K^+$  ratios of above one, i.e., a chemical  
353 signature for apparent impacts of agricultural fires, were found to have LG/OC ratios larger than  
354 2%. In addition, LG/OC ratio could also work as an estimate of the strength of biomass burning  
355 impact. Thus in the following discussions, LG/OC of > 2% was used as an indicator for open burning  
356 episodes and correspondingly, spring samples with LG/OC of below 2% were referred to as typical  
357 ones.  $MAE_{365}$  averaged  $0.80 \pm 0.22$  m<sup>2</sup>/gC for the typical samples of spring, lower than results from  
358 the winter campaign ( $1.55 \pm 0.18$  m<sup>2</sup>/gC; Figure S4a). This seasonal pattern coincided with the  
359 overall lower  $R_{S/N}$  in spring (Figure S4b). It was unlikely that the number of in-use vehicles or the  
360 fleet composition in Harbin could vary significantly between January and April of the same year.  
361 Thus the reduced springtime  $R_{S/N}$ , i.e., the relatively low  $MAE_{365}$  with the absence of agricultural  
362 fires, should be caused mainly by the decrease of coal combustion emissions, e.g., due to the less  
363 demand for heating.

### 364 **3.3 Unique wavelength dependence of BrC absorption during agricultural fire episodes**

365 The agricultural fires not only elevated  $MAE_{365}$  but also changed the wavelength dependence  
366 of brown carbon. For the wavelength range used for AAE calculation (310–460 nm), the detection  
367 limit of optical attenuation ( $ATN_{LOD}$ ) was ~0.02, which was determined as three times the maximum  
368 standard deviation of parallel  $ATN_{\lambda}$  results from blank filters. Before further discussions, we

369 introduced a new term “relative  $\ln(ATN_\lambda)$ ”, i.e.,  $\ln(ATN_\lambda)^*$  calculated as  $\ln(ATN_\lambda) - \ln(ATN_{LOD})$ .  
 370 A benefit of using the new term was that a  $\ln(ATN_\lambda)^*$  value of zero corresponded to  $ATN_\lambda = ATN_{LOD}$   
 371 and thus  $\ln(ATN_\lambda)^*$  could be considered “real” absorption by chromophores in solutions. It should  
 372 be noted that the use of  $\ln(ATN_\lambda)^*$  would not influence the determination of AAE, since the same  
 373 slope would be derived from the regressions of  $\ln(ATN_\lambda)^*$  and  $\ln(ATN_\lambda)$  on  $\ln(\lambda)$ . For the typical  
 374 samples of spring, the dependence of  $\ln(ATN_\lambda)^*$  on  $\ln(\lambda)$  could be properly approximated by a linear  
 375 function, usually with  $r$  values of above 0.995. In this case, AAE could be reliably determined, and  
 376 an average value of  $6.92 \pm 0.28$  was obtained.

377 The relationship between  $\ln(ATN_\lambda)^*$  and  $\ln(\lambda)$  became non-linear for the open burning episodes.  
 378 To more quantitatively describe the non-linearity, we added an “auxiliary line” to each measured  
 379 spectrum (Figure 6a), by drawing a line between the two points with  $x$  values of  $\ln(310)$  and  $\ln(460)$ .  
 380 The “auxiliary line” could be considered an assumed spectrum with linear dependence of  $\ln(ATN_\lambda)^*$   
 381 on  $\ln(\lambda)$ . The measured spectrum was always above the assumed one and their largest difference  
 382 was typically observed at  $\sim 365$  nm, pointing to the presence of distinct BrC chromophores with  
 383 absorption peak around this wavelength.

384 The influence of such chromophores on BrC absorption could be estimated by the following  
 385 three indicators. The first one ( $F$ ) was related to the difference between the measured and assumed  
 386  $\ln(ATN_\lambda)^*$  at 365 nm:

387 
$$F = \left[ \ln(ATN_{365})_m^* - \ln(ATN_{365})_a^* \right] / \ln(ATN_{365})_a^*$$
, where the subscripts “m” and “a” indicate

388 results from the measured and assumed spectra, respectively (Figure 6a). The second indicator ( $K$ )  
 389 was related to the area enclosed between the two spectra ( $S_2$ ):  $K = S_2/S_1$ , where  $S_1$  indicates the area  
 390 enclosed by the assumed spectrum and  $x$ -axis (Figure 6b). The last indicator was  $\Delta(b_{abs})_{365}$

391 calculated as  $(b_{\text{abs}})_{365}^{\text{m}} - (b_{\text{abs}})_{365}^{\text{a}}$ , where the superscripts “m” and “a” indicate absorption  
392 coefficients calculated based on the measured and assumed spectra, respectively.  $F$  and  $K$  exhibited  
393 a strong linear correlation for the open burning episodes ( $r = 0.99$ ; Figure 6c), indicating that the  
394 differences between the measured and assumed spectra were likely caused by the same class of BrC  
395 compounds. In addition, these compounds could be primarily traced back to biomass burning, since  
396  $\Delta(b_{\text{abs}})_{365}$  showed a positive dependence on LG/OC (Figure 6d). Candidates for such compounds  
397 were aromatic species with nitro-functional groups, based on a synthesis of absorption spectra  
398 measured for various BrC chromophores (Huang et al., 2020) and molecular characterization results  
399 for biomass burning emissions (Lin et al., 2016, 2017; Xie et al., 2019, 2020). Chamber experiments  
400 by Iinuma et al. (2010) suggested that aromatic compounds with nitro-functional groups could also  
401 be formed through photooxidation of gaseous precursors emitted by biomass burning (*m*-cresol). In  
402 this study, however, all the samples with relatively high  $\Delta(b_{\text{abs}})_{365}$  levels (e.g., above  $20 \text{ Mm}^{-1}$ ) were  
403 collected at night, indicating that the distinct BrC chromophores with absorption peak at  $\sim 365 \text{ nm}$   
404 were more strongly associated with primary emissions from agricultural fires. In addition, the  
405 chromophores seemed to be subject to photo-bleaching, as both  $F$  and  $K$  decreased substantially (by  
406  $\sim 65\%$ ) during the day compared to the nighttime results (Figure 7).

407 For the open burning episodes, the distinct absorption peak at  $\sim 365 \text{ nm}$  prohibited a proper  
408 determination of AAE. If enforcing a linear function for the dependence of  $\ln(\text{ATN}_{\lambda})^*$  on  $\ln(\lambda)$ , lower  
409  $r$  values would be derived (down to  $\sim 0.97$ , with an average of  $0.992 \pm 0.007$ ) compared to the typical  
410 samples (averaging  $0.998 \pm 0.002$ ). In addition,  $r$  showed decreasing trends with the increases of  
411 LG/OC (Figure 6e) and  $F$  (Figure S5), suggesting that the relationship between  $\ln(\text{ATN}_{\lambda})^*$  and  $\ln(\lambda)$   
412 deviated more significantly from linearity as the  $\sim 365 \text{ nm}$  absorption peak, i.e., the influence of

413 agricultural fires, became more significant. We suggest that for the open burning episodes, the AAE  
414 results should be interpreted with caution, although they could be calculated mathematically with  
415 reasonable  $r$  values (e.g., even the minimum  $r$  appeared acceptable).

#### 416 **3.4 Diurnal variations of wintertime AAE**

417 Similar to the typical samples of spring,  $\ln(\text{ATN}_\lambda)^*$  exhibited linear dependences on  $\ln(\lambda)$  for  
418 all the winter samples. The wintertime AAE were higher at night compared to those observed during  
419 the day (with averages of  $7.33 \pm 0.14$  and  $6.76 \pm 0.11$ , respectively; 2-tailed  $p = 0.000$ ), consistent  
420 with the pattern observed during winter in Beijing (Li et al., 2020). The relative abundance of  
421 secondary OC (SOC) has been considered an important influencing factor for AAE, e.g., an  
422 increasing trend was observed for AAE during long-range transport of BrC over the Indo-Gangetic  
423 Plain (Dasari et al., 2019). Although SOC or its organic tracer was not determined in this study,  
424 previous source apportionment results from Harbin (based on PMF) showed a strong correlation  
425 between SOC and sulfate, with largely consistent relationships among different campaigns (Cheng  
426 et al., 2022b). Thus we used sulfate as an indicator for SOC. During the winter campaign, the sulfate  
427 to OC ratios were lower at night (averaging 0.38, compared to 0.44 during the day; 2-tailed  $p =$   
428 0.011), pointing to decreased fractions of SOC in OC. This inference was consistent with the higher  
429 LG/OC and  $R_{S/N}$  levels observed at night, which had been attributed to increased emissions from  
430 residential biomass burning and vehicular exhausts, respectively. Thus regarding the association  
431 between AAE and SOC formation, results from the winter campaign were inconsistent with Dasari  
432 et al. (2019), but the reason remained unclear. Molecular characterization of organic aerosols should  
433 be necessary to unfold the response of AAE to changes in BrC sources.

#### 434 **4. Conclusions**

435 Diurnal variations of BrC were investigated during two distinct seasons in the northernmost  
436 megacity in China. The winter campaign was characterized by low temperatures rarely seen in other  
437 hotspots of air pollution studies such as the North China Plain. The wintertime BrC aerosols were  
438 slightly more absorbing at night, with an average MAE<sub>365</sub> of  $1.61 \pm 0.15 \text{ m}^2/\text{gC}$  compared to  $1.48 \pm$   
439  $0.18 \text{ m}^2/\text{gC}$  during the day. Various indicators were used to explain the observed diurnal variations  
440 of MAE<sub>365</sub>, including those associated with biomass burning emissions (LG/K<sup>+</sup> and LG/OC),  
441 relative importance of coal combustion and vehicle emissions ( $R_{S/N}$ ) and secondary aerosol  
442 formation (SOR and NOR). For the winter campaign, the nighttime samples were characterized by  
443 increased BB emissions from residential sources, enhanced heterogeneous chemistry and weakened  
444 photochemical reactions. But none of these factors was identified as the dominant driver for the  
445 higher MAE<sub>365</sub> at night. Instead, MAE<sub>365</sub> exhibited a negative dependence on  $R_{S/N}$ , and the lower  
446  $R_{S/N}$  and thus higher MAE<sub>365</sub> at night were primarily attributed to increased emissions from heavy-  
447 duty diesel trucks, which were not allowed in the main urban area during the day. In addition, the  
448 wintertime AAE were higher at night but it remained difficult to unfold the underlying connection  
449 between this diurnal pattern and the changes in BrC sources.

450 The spring campaign was characterized by frequent occurrences of agricultural fires, with more  
451 pronounced diurnal variations of MAE<sub>365</sub> (averaging  $0.98 \pm 0.31$  and  $1.69 \pm 0.65 \text{ m}^2/\text{gC}$  for the  
452 daytime and nighttime samples, respectively). Unlike winter, the springtime MAE<sub>365</sub> were mainly  
453 influenced by open burning emissions, as suggested by the positive dependence of MAE<sub>365</sub> on  
454 LG/OC and the lack of correlation between MAE<sub>365</sub> and  $R_{S/N}$ . The higher nighttime LG/OC  
455 indicated that the farmers preferred burning the crop residues at night, presumably because  
456 agricultural fires were nominally prohibited by the local government. In addition, BrC exhibited

457 distinct light absorption spectra during agricultural fire episodes, as indicated by the non-linear  
458 relationship between  $\ln(ATN_\lambda)^*$  on  $\ln(\lambda)$ . The non-linearity was mainly caused by chromophores  
459 with absorption peak at  $\sim 365$  nm, which became more significant with increasing BB influence.  
460 Aromatic species with nitro-functional groups were a possible class of compounds that were at play.  
461 The presence of such chromophores, i.e., the distinct absorption peak at  $\sim 365$  nm, prohibited a  
462 proper determination of AAE for the spring samples impacted by agricultural fires.

## 463 **5. Implications**

464  $MAE_{365}$  and AAE are key parameters for simulating climate effects of brown carbon. In winter,  
465 although Harbin experiences low temperatures rarely seen in other Chinese megacities, the observed  
466  $MAE_{365}$  and AAE were largely comparable with the typical results from other regions in Northern  
467 China (e.g., Beijing; Cheng et al., 2016). In addition, BrC's optical properties were indeed different  
468 between daytime and nighttime samples, which were likely associated with increased HDDT  
469 emissions at night. However, the diurnal variations ( $\sim 10\%$  higher at night for both  $MAE_{365}$  and AAE)  
470 appeared negligible compared to uncertainties in simulating the mass concentration of BrC, i.e.,  
471 organic aerosol. Thus for typical winter conditions in Northern China (without open burning), it  
472 may be practical to use fixed  $MAE_{365}$  and AAE values for estimating the wavelength-resolved  
473 absorption by organic aerosol in climate models.

474 The spring campaign suggested another scenario, that the agricultural fires exhibited strong  
475 influences on optical properties of brown carbon, as highlighted by the  $\sim 365$  nm peak in BrC's  
476 absorption spectra. The distinct peak on one hand effectively elevated  $MAE_{365}$ , and on the other  
477 hand complicated the determination of AAE. In addition, the peak became less significant during  
478 the day, indicating that the organic compounds at play were likely subject to photo-bleaching. BrC

479 emitted by the fires remained difficult to constrain, partially due to the variable combustion  
480 efficiencies. This in turn resulted in challenges for simulating climate effects of the open burning  
481 aerosols. Given the massive agricultural sector in Northeast China, more studies are necessary to  
482 understand the emissions, transformation and impacts of the fire-induced pollutants.

483 **Data availability.** Data described in this manuscript can be accessed at  
484 <https://doi.org/10.5281/zenodo.7874760> (Cheng, 2023).

485 **Author contributions.** YC and JL designed the study and prepared the paper with inputs from all  
486 the co-authors. XC, YZ and QY carried out the experiments. QZ and KH validated the results and  
487 supervised the study.

488 **Competing interests.** Author Qiang Zhang is a member of the editorial board of *Atmospheric*  
489 *Chemistry and Physics*. The peer-review process was guided by an independent editor, and the  
490 authors have also no other competing interests to declare.

491 **Acknowledgements.** The authors thank Zhen-yu Du at National Research Center for Environmental  
492 Analysis and Measurement, and Lin-lin Liang at Chinese Academy of Meteorological Sciences for  
493 their help in sample analysis.

494 **Financial support.** This research has been supported by the National Natural Science Foundation  
495 of China (42222706), the Natural Science Foundation of Heilongjiang Province (LH2020D011),  
496 Fundamental Research Funds for the Central Universities, and Heilongjiang Touyan Team.

## 497 **References**

498 Akagi, S. K., Craven, J. S., Taylor, J. W., McMeeking, G. R., Yokelson, R. J., Burling, I. R., Urbanski,  
499 S. P., Wold, C. E., Seinfeld, J. H., Coe, H., Alvarado, M. J., and Weise, D. R.: Evolution of  
500 trace gases and particles emitted by a chaparral fire in California, *Atmos. Chem. Phys.*, 12,  
501 1397–1421, <https://doi.org/10.5194/acp-12-1397-2012>, 2012.  
502 Brege, M. A., China, S., Schum, S., Zelenyuk, A., and Mazzoleni, L. R.: Extreme molecular

503 complexity resulting in a continuum of carbonaceous species in biomass burning tar balls from  
504 wildfire smoke, *ACS Earth Space Chem.*, 5, 2729–2739,  
505 <https://doi.org/10.1021/acsearthspacechem.1c00141>, 2015.

506 Brown, H., Liu, X. H., Feng, Y., Jiang, Y. Q., Wu, M. X., Lu, Z., Wu, C. L., Murphy, S., and Pokhrel,  
507 R.: Radiative effect and climate impacts of brown carbon with the Community Atmosphere  
508 Model (CAM5), *Atmos. Chem. Phys.*, 18, 17745–17768, [https://doi.org/10.5194/acp-18-](https://doi.org/10.5194/acp-18-17745-2018)  
509 17745-2018, 2018.

510 Cappa, C. D., Lim, C. Y., Hagan, D. H., Coggon, M., Koss, A., Sekimoto, K., de Gouw, J., Onasch,  
511 T. B., Warneke, C., and Kroll, J. H.: Biomass-burning-derived particles from a wide variety of  
512 fuels – Part 2: effects of photochemical aging on particle optical and chemical properties,  
513 *Atmos. Chem. Phys.*, 20, 8511–8532, <https://doi.org/10.5194/acp-20-8511-2020>, 2020.

514 Chen, X. R., Wang, H. C., Lu, K. D., Li, C. M., Zhai, T. Y., Tan, Z. F., Ma, X. F., Yang, X. P., Liu,  
515 Y. H., Chen, S. Y., Dong, H. B., Li, X., Wu, Z. J., Hu, M., Zeng, L. M., and Zhang, Y. H.: Field  
516 determination of nitrate formation pathway in winter Beijing, *Environ. Sci. Technol.*, 54,  
517 9243–9253, <https://doi.org/10.1021/acs.est.0c00972>, 2020.

518 Chen, Y., and Bond, T. C.: Light absorption by organic carbon from wood combustion, *Atmos.*  
519 *Chem. Phys.*, 10, 1773–1787, <https://doi.org/10.5194/acp-10-1773-2010>, 2010.

520 Cheng, Y.: Diurnal variations of brown carbon during two distinct seasons in a megacity in  
521 Northeast China [data set], <https://doi.org/10.5281/zenodo.7874760>, 2023.

522 Cheng, Y., He, K. B., Du, Z. Y., Engling, G., Liu, J. M., Ma, Y. L., Zheng, M., and Weber, R. J.: The  
523 characteristics of brown carbon aerosol during winter in Beijing, *Atmos. Environ.*, 127, 355–  
524 364, <https://doi.org/10.1016/j.atmosenv.2015.12.035>, 2016.

525 Cheng, Y., Cao, X. B., Liu, J. M., Yu, Q. Q., Wang, P., Yan, C. Q., Du, Z. Y., Liang, L. L., Zhang,  
526 Q., and He, K. B.: Primary nature of brown carbon absorption in a frigid atmosphere with  
527 strong haze chemistry, *Environ. Res.*, 204, 112324,  
528 <https://doi.org/10.1016/j.envres.2021.112324>, 2022a.

529 Cheng, Y., Cao, X. B., Liu, J. M., Yu, Q. Q., Zhong, Y. J., Geng, G. N., Zhang, Q., and He, K. B.:  
530 New open burning policy reshaped the aerosol characteristics of agricultural fire episodes in  
531 Northeast China, *Sci. Total Environ.*, 810, 152272,  
532 <https://doi.org/10.1016/j.scitotenv.2021.152272>, 2022b.

533 Chu, B. W., Zhang, S. P., Liu, J., Ma, Q. X., and He, H.: Significant concurrent decrease in PM<sub>2.5</sub>  
534 and NO<sub>2</sub> concentrations in China during COVID-19 epidemic, *J. Environ. Sci.*, 99, 346–353,  
535 <https://doi.org/10.1016/j.jes.2020.06.031>, 2021.



536 Dallmann, T. R., DeMartini, S. J., Kirchstetter, T. W., Herndon, S. C., Onasch, T. B., Wood, E. C.,  
537 and Harley, R. A.: On-road measurement of gas and particle phase pollutant emission factors  
538 for individual heavy-duty diesel trucks, *Environ. Sci. Technol.*, 46, 8511–8518,  
539 <https://doi.org/10.1021/es301936c>, 2012.

540 Dasari, S., Andersson, A., Bikkina, S., Holmstrand, H., Budhavant, K., Satheesh, S., Asmi, E., Kesti,  
541 J., Backman, J., Salam, A., Bisht, D. S., Tiwari, S., Hameed, Z., and Gustafsson, Ö.:  
542 Photochemical degradation affects the light absorption of water-soluble brown carbon in the  
543 South Asian outflow, *Sci. Adv.*, 5, eaau8066, <https://doi.org/10.1126/sciadv.aau8066>, 2019.

544 Du, W., Shen, G. F., Chen, Y. C., Zhu, X., Zhuo, S. J., Zhong, Q. R., Qi, M., Xue, C. Y., Liu, G. Q.,  
545 Zeng, E., Xing, B. S., and Tao, S.: Comparison of air pollutant emissions and household air  
546 quality in rural homes using improved wood and coal stoves, *Atmos. Environ.*, 166, 215–223,  
547 <https://doi.org/10.1016/j.atmosenv.2017.07.029>, 2017.

548 Engling, G., Carrico, C. M., Kreidenweis, S. M., Collett Jr, J. L., Day, D. E., Malm, W. C., Lincoln,  
549 L., Hao, W. M., Iinuma, Y., and Herrmann, H.: Determination of levoglucosan in biomass  
550 combustion aerosol by high-performance anion-exchange chromatography with pulsed  
551 amperometric detection, *Atmos. Environ.*, 40, S299–S311,  
552 <https://doi.org/10.1016/j.atmosenv.2005.12.069>, 2006.

553 Gao, S., Hegg, D. A., Hobbs, P. V., Kirchstetter, T. W., Magi, B. I., and Sadilek, M.: Water-soluble  
554 organic components in aerosols associated with savanna fires in southern Africa: identification,  
555 evolution, and distribution, *J. Geophys. Res.*, 108, D13, 8491,  
556 <https://doi.org/10.1029/2002JD002324>, 2003.

557 Hecobian, A., Zhang, X., Zheng, M., Frank, N., Edgerton, E. S., and Weber, R. J.: Water-soluble  
558 organic aerosol material and the light-absorption characteristics of aqueous extracts measured  
559 over the Southeastern United States, *Atmos. Chem. Phys.*, 10, 5965–5977,  
560 <https://doi.org/10.5194/acp-10-5965-2010>, 2010.

561 Huang, R. J., Yang, L., Shen, J. C., Yuan, W., Gong, Y. Q., Guo, J., Cao, W. J., Duan, J., Ni, H. Y.,  
562 Zhu, C. S., Dai, W. T., Li, Y. J., Chen, Y., Chen, Q., Wu, Y. F., Zhang, R. J., Dusek, U., and  
563 O'Dowd, C.: Water-Insoluble organics dominate brown carbon in wintertime urban aerosol of  
564 China: chemical characteristics and optical properties, *Environ. Sci. Technol.*, 54, 7836–7847,  
565 <https://doi.org/10.1021/acs.est.0c01149>, 2020.

566 Huang, R. J., Yang, L., Shen, J. C., Yuan, W., Gong, Y. Q., Ni, H. Y., Duan, J., Yan, J., Huang, H.  
567 B., You, Q. H., and Li, Y. J.: Chromophoric fingerprinting of brown carbon from residential  
568 biomass burning, *Environ. Sci. Technol. Lett.*, 9, 102–111,  
569 <https://doi.org/10.1021/acs.estlett.1c00837>, 2022.

570 Huo, Y. Q., Guo, Z. H., Li, Q., Wu, D., Ding, X., Liu, A. L., Huang, D., Qiu, G. K., Wu, M. M.,  
571 Zhao, Z. J., Sun, H., Song, W. H., Li, X., Chen, Y. J., Wu, T. C., and Chen, J. M.: Chemical  
572 fingerprinting of HULIS in particulate matters emitted from residential coal and biomass  
573 combustion, *Environ. Sci. Technol.*, 55, 3593–3603,  
574 <https://doi.org/10.1021/acs.est.0c08518>, 2021.

575 Iinuma, Y., Böge, O., Gräfe, R., and Herrmann, H.: Methyl-nitrocatechols: atmospheric tracer  
576 compounds for biomass burning secondary organic aerosols, *Environ. Sci. Technol.*, 44, 8453–  
577 8459, <https://doi.org/10.1021/es102938a>, 2010.

578 Jiang, H. X., Li, J., Sun, R., Tian, C. G., Tang, J., Jiang, B., Liao, Y. H., Chen, C. E., and Zhang, G.:  
579 Molecular dynamics and light absorption properties of atmospheric dissolved organic matter,  
580 *Environ. Sci. Technol.*, 55, 10268–10279, <https://doi.org/10.1021/acs.est.1c01770>, 2021.

581 Kumar, N. K., Corbin, J. C., Bruns, E. A., Massabó, D., Slowik, J. G., Drinovec, L., Močnik, G.,  
582 Prati, P., Vlachou, A., Baltensperger, U., Gysel, M., El-Haddad, I., and Prévôt, A. S. H.:  
583 Production of particulate brown carbon during atmospheric aging of residential wood-burning  
584 emissions, *Atmos. Chem. Phys.*, 18, 17843–17861, [https://doi.org/10.5194/acp-18-17843-](https://doi.org/10.5194/acp-18-17843-2018)  
585 2018, 2018.

586 Lack, D. A., Langridge, J. M., Bahreini, R., Cappa, C. D., Middlebrook, A. M., and Schwarz, J. P.:  
587 Brown carbon and internal mixing in biomass burning particles, *Proc. Natl. Acad. Sci. USA*,  
588 109, 14802–14807, <https://doi.org/10.1073/pnas.1206575109>, 2012.

589 Laskin, A., Laskin, J., and Nizkorodov, S. A.: Chemistry of atmospheric brown carbon, *Chem. Rev.*,  
590 115, 4335–4382, <https://doi.org/10.1021/cr5006167>, 2015.

591 Li, M., Liu, H., Geng, G. N., Hong, C. P., Liu, F., Song, Y., Tong, D., Zheng, B., Cui, H. Y., Man,  
592 H. Y., Zhang, Q., and He, K. B.: Anthropogenic emission inventories in China: a review, *Natl.*  
593 *Sci. Rev.*, 4, 834–866, <https://doi.org/10.1093/nsr/nwx150>, 2017.

594 Li, X., Wang, Y. J., Hu, M., Tan, T. Y., Li, M. R., Wu, Z. J., Chen, S. Y., and Tang, X. Y.:  
595 Characterizing chemical composition and light absorption of nitroaromatic compounds in the  
596 winter of Beijing, *Atmos. Environ.*, 237, 117712,  
597 <https://doi.org/10.1016/j.atmosenv.2020.117712>, 2019.

598 Li, Y. C., Liu, J., Han, H., Zhao, T. L., Zhang, X., Zhuang, B. L., Wang, T. J., Chen, H. M., Wu, Y.,  
599 and Li, M. M.: Collective impacts of biomass burning and synoptic weather on surface PM<sub>2.5</sub>  
600 and CO in Northeast China, *Atmos. Environ.*, 213, 64–80,  
601 <https://doi.org/10.1016/j.atmosenv.2019.05.062>, 2019.

602 Li, Y. R., Tan, Z. Q., Ye, C. X., Wang, J. X., Wang, Y. W., Zhu, Y., Liang, P. F., Chen, X., Fang, Y.

603 H., Han, Y. Q., Wang, Q., He, D., Wang, Y., and Zhu, T.: Using wavelet transform to analyse  
604 on-road mobile measurements of air pollutants: a case study to evaluate vehicle emission  
605 control policies during the 2014 APEC summit, *Atmos. Chem. Phys.*, 19, 13841–13857,  
606 <https://doi.org/10.5194/acp-19-13841-2019>, 2019.

607 Lian, X. B., Huang, J. P., Huang, R. J., Liu, C. W., Wang, L. N., and Zhang, T. H.: Impact of city  
608 lockdown on the air quality of COVID-19-hit of Wuhan city, *Sci. Total Environ.*, 742, 140556,  
609 <https://doi.org/10.1016/j.scitotenv.2020.140556>, 2020.

610 Lin, P., Aiona, P. K., Li, Y., Shiraiwa, M., Laskin, J., Nizkorodov, S. A., and Laskin, A.: Molecular  
611 characterization of brown carbon in biomass burning aerosol particles, *Environ. Sci. Technol.*,  
612 50, 11815–11824, <https://doi.org/10.1021/acs.est.6b03024>, 2016.

613 Lin, P., Bluvshstein, N., Rudich, Y., Nizkorodov, S. A., Laskin, J., and Laskin, A.: Molecular  
614 chemistry of atmospheric brown carbon inferred from a nationwide biomass burning event,  
615 *Environ. Sci. Technol.*, 51, 11561–11570, <https://doi.org/10.1021/acs.est.7b02276>, 2017.

616 Lin, P., Fleming, L. T., Nizkorodov, S. A., Laskin, J., and Laskin, A.: Comprehensive molecular  
617 characterization of atmospheric brown carbon by high resolution mass spectrometry with  
618 electrospray and atmospheric pressure photoionization, *Anal. Chem.*, 90, 12493–12502,  
619 <https://doi.org/10.1021/acs.analchem.8b02177>, 2018.

620 Lin, P., Laskin, J., Nizkorodov, S. A., and Laskin, A.: Revealing brown carbon chromophores  
621 produced in reactions of methylglyoxal with ammonium sulfate, *Environ. Sci. Technol.*, 49,  
622 14257–14266, <https://doi.org/10.1021/acs.est.5b03608>, 2015.

623 Liu, T. Y., Chan, A. W. H., and Abbatt, J. P. D.: Multiphase oxidation of sulfur dioxide in aerosol  
624 particles: implications for sulfate formation in polluted environments, *Environ. Sci. Technol.*,  
625 8, 4227–4242, <https://doi.org/10.1021/acs.est.0c06496>, 2021.

626 Liu, X. X., Zhang, Y., Huey, L. G., Yokelson, R. J., Wang, Y., Jimenez, J. L., Campuzano-Jost, P.,  
627 Beyersdorf, A. J., Blake, D. R., Choi, Y., St Clair, J. M., Crouse, J. D., Day, D. A., Diskin, G.  
628 S., Fried, A., Hall, S. R., Hanisco, T. F., King, L. E., Meinardi, S., Mikoviny, T., Palm, B. B.,  
629 Peischl, J., Perring, A. E., Pollack, I. B., Ryerson, T. B., Sachse, G., Schwarz, J. P., Simpson, I.  
630 J., Tanner, D. J., Thornhill, K. L., Ullmann, K., Weber, R. J., Wennberg, P. O., Wisthaler, A.,  
631 Wolfe, G. M., and Ziemba, L. D.: Agricultural fires in the southeastern U.S. during SEAC<sup>4</sup>RS:  
632 emissions of trace gases and particles and evolution of ozone, reactive nitrogen, and organic  
633 aerosol, *J. Geophys. Res. Atmos.*, 121, 7383–7414, <https://doi.org/10.1002/2016JD025040>,  
634 2016.

635 McClure, C. D., Lim, C. Y., Hagan, D. H., Kroll, J. H., and Cappa, C. D.: Biomass-burning-derived  
636 particles from a wide variety of fuels – Part 1: properties of primary particles, *Atmos. Chem.*

637 *Phys.*, 20, 1531–1547, <https://doi.org/10.5194/acp-20-1531-2020>, 2020.

638 McMeeking, G. R., Kreidenweis, S. M., Baker, S., Carrico, C. M., Chow, J. C., Collett Jr., J. L.,  
639 Hao, W. M., Holden, A. S., Kirchstetter, T. W., Malm, W. C., Moosmüller, H., Sullivan, A. P.,  
640 and Wold, C. E.: Emissions of trace gases and aerosols during the open combustion of biomass  
641 in the laboratory, *J. Geophys. Res.*, 114, D19210, <https://doi.org/10.1029/2009JD011836>, 2009.

642 Mohr, C., Lopez-Hilfiker, F. D., Zotter, P., Prévôt, A. S. H., Xu, L., Ng, N. L., Herndon, S. C.,  
643 Williams, L. R., Franklin, J. P., Zahniser, M. S., Worsnop, D. R., Knighton, W. B., Aiken, A.  
644 C., Gorkowski, K. J., Dubey, M. K., Allan, J. D., and Thornton, J. A.: Contribution of nitrated  
645 phenols to wood burning brown carbon light absorption in Detling, United Kingdom during  
646 winter time, *Environ. Sci. Technol.*, 47, 6316–6324, <https://doi.org/10.1021/es400683v>, 2013.

647 Ni, H. Y., Huang, R. J., Pieber, S. M., Corbin, J. C., Stefenelli, G., Pospisilova, V., Klein, F., Gysel-  
648 Beer, M., Yang, L., Baltensperger, U., El Haddad, I., Slowik, J. G., Cao, J. J., Prévôt, A. S. H.,  
649 and Dusek, U.: Brown carbon in primary and aged coal combustion emission, *Environ. Sci.*  
650 *Technol.*, 55, 5701–5710, <https://doi.org/10.1021/acs.est.0c08084>, 2021.

651 Pokhrel, R. P., Wagner, N. L., Langridge, J. M., Lack, D. A., Jayarathne, T., Stone, E. A., Stockwell,  
652 C. E., Yokelson, R. J., and Murphy, S. M.: Parameterization of single-scattering albedo (SSA)  
653 and absorption Ångström exponent (AAE) with EC/OC for aerosol emissions from biomass  
654 burning, *Atmos. Chem. Phys.*, 16, 9549–9561, <https://doi.org/10.5194/acp-16-9549-2016>,  
655 2016.

656 Saleh, R.: From measurements to models: toward accurate representation of brown carbon in climate  
657 calculations, *Curr. Pollut. Rep.*, 6, 90–104, <https://doi.org/10.1007/s40726-020-00139-3>, 2020.

658 Salvador, C. M. G., Tang, R. Z., Priestley, M., Li, L. J., Tsiligiannis, E., Le Breton, M., Zhu, W. F.,  
659 Zeng, L. M., Wang, H., Yu, Y., Hu, M., Guo, S., and Hallquist, M.: Ambient nitro-aromatic  
660 compounds – biomass burning versus secondary formation in rural China, *Atmos. Chem. Phys.*,  
661 21, 1389–1406, <https://doi.org/10.5194/acp-21-1389-2021>, 2021.

662 Sand, M., Samset, B. H., Myhre, G., Gliß, J., Bauer, S. E., Bian, H. S., Chin, M., Checa-Garcia, R.,  
663 Ginoux, P., Kipling, Z., Kirkevåg, A., Kokkola, H., Le Sager, P., Lund, M. T., Matsui, H., van  
664 Noije, T., Olivieri, D. J. L., Remy, S., Schulz, M., Stier, P., Stjern, C. W., Takemura, T., Tsigaridis,  
665 K., Tsyro, S. G., and Watson-Parris, D.: Aerosol absorption in global models from AeroCom  
666 phase III, *Atmos. Chem. Phys.*, 21, 15929–15947, <https://doi.org/10.5194/acp-21-15929-2021>,  
667 2021.

668 Shen, X. B., Hao, J. T., Kong, L., Shi, Y., Cao, X. Y., Shi, J. C., Yao, Z. L., Li, X., Wu, B. B., Xu, Y.  
669 M., and He, K. B.: Variation characteristics of fine particulate matter and its components in  
670 diesel vehicle emission plumes, *J. Environ. Sci.*, 107, 138–149,

671 <https://doi.org/10.1016/j.jes.2021.01.034>, 2021.

672 Su, H., Cheng, Y. F., and Pöschl, U.: New multiphase chemical processes influencing atmospheric  
673 aerosols, air quality, and climate in the Anthropocene, *Acc. Chem. Res.*, 53, 2034–2043,  
674 <https://doi.org/10.1021/acs.accounts.0c00246>, 2020.

675 Tabazadeh, A., Djikaev, Y. S., and Reiss, H.: Surface crystallization of supercooled water in clouds,  
676 *Proc. Natl. Acad. Sci. USA*, 99, 15873–15878, <https://doi.org/10.1073/pnas.252640699>, 2002.

677 Wang, Q. Q., Zhou, Y. Y., Ma, N., Zhu, Y., Zhao, X. C., Zhu, S. W., Tao, J. C., Hong, J., Wu, W. J.,  
678 Cheng, Y. F., and Su, H.: Review of brown carbon aerosols in China: pollution level, optical  
679 properties, and emissions, *J. Geophys. Res. Atmos.*, 127, e2021JD035473,  
680 <https://doi.org/10.1029/2021JD035473>, 2022.

681 Wang, Y. S., Li, W. J., Gao, W. K., Liu, Z. R., Tian, S. L., Shen, R. R., Ji, D. S., Wang, S., Wang, L.  
682 L., Tang, G. Q., Song, T., Cheng, M. T., Wang, G. H., Gong, Z. Y., Hao, J. M., and Zhang, Y.  
683 H.: Trends in particulate matter and its chemical compositions in China from 2013-2017, *Sci.  
684 China Earth Sci.*, 62, 1857–1871, <https://doi.org/10.1007/s11430-018-9373-1>, 2019.

685 Washenfelder, R. A., Azzarello, L., Ball, K., Brown, S. S., Decker, Z. C. J., Franchin, A.,  
686 Fredrickson, C. D., Hayden, K., Holmes, C. D., Middlebrook, A. M., Palm, B. B., Pierce, R.  
687 B., Price, D. J., Roberts, J. M., Robinson, M. A., Thornton, J. A., Womack, C. C., and Young,  
688 C. J.: Complexity in the evolution, composition, and spectroscopy of brown carbon in aircraft  
689 measurements of wildfire plumes, *Geophys. Res. Lett.*, 49, e2022GL098951,  
690 <https://doi.org/10.1029/2022GL098951>, 2022.

691 Wozniak, A. S., Bauer, J. E., Sleighter, R. L., Dickhut, R. M., and Hatcher, P. G.: Technical Note:  
692 Molecular characterization of aerosol-derived water soluble organic carbon using ultrahigh  
693 resolution electrospray ionization Fourier transform ion cyclotron resonance mass  
694 spectrometry, *Atmos. Chem. Phys.*, 8, 5099–5111, <https://doi.org/10.5194/acp-8-5099-2008>,  
695 2008.

696 Wu, J., Kong, S. F., Yan, Y. Y., Yao, L. Q., Yan, Q., Liu, D. T., Shen, G. F., Zhang, X. Y., and Qi, S.  
697 H.: Neglected biomass burning emissions of air pollutants in China-views from the corncob  
698 burning test, emission estimation, and simulations, *Atmos. Environ.*, 278, 119082,  
699 <https://doi.org/10.1016/j.atmosenv.2022.119082>, 2022.

700 Xie, M. J., Chen, X., Hays, M. D., and Holder, A. L.: Composition and light absorption of N-  
701 containing aromatic compounds in organic aerosols from laboratory biomass burning, *Atmos.  
702 Chem. Phys.*, 19, 2899–2915, <https://doi.org/10.5194/acp-19-2899-2019>, 2019.

703 Xie, M. J., Zhao, Z. Z., Holder, A. L., Hays, M. D., Chen, X., Shen, G. F., Jetter, J. J., Champion,

704 W. M., and Wang, Q. G.: Chemical composition, structures, and light absorption of N-  
705 containing aromatic compounds emitted from burning wood and charcoal in household  
706 cookstoves, *Atmos. Chem. Phys.*, 20, 14077–14090, [https://doi.org/10.5194/acp-20-14077-](https://doi.org/10.5194/acp-20-14077-2020)  
707 2020, 2020.

708 Xu, J. Z., Hettiyadura, A. P. S., Liu, Y. M., Zhang, X. H., Kang, S. C., and Laskin, A.: Atmospheric  
709 brown carbon on the Tibetan Plateau: regional differences in chemical composition and light  
710 absorption properties, *Environ. Sci. Technol. Lett.*, 9, 219–225,  
711 <https://doi.org/10.1021/acs.estlett.2c00016>, 2022.

712 Yang, M., Howell, S. G., Zhuang, J., and Huebert, B. J.: Attribution of aerosol light absorption to  
713 black carbon, brown carbon, and dust in China - Interpretations of atmospheric measurements  
714 during EAST-AIRE, *Atmos. Chem. Phys.*, 9, 2035–2050, [https://doi.org/10.5194/acp-9-2035-](https://doi.org/10.5194/acp-9-2035-2009)  
715 2009, 2009.

716 Yttri, K. E., Schnelle-Kreis, J., Maenhaut, W., Abbaszade, G., Alves, C., Bjerke, A., Bonnier, N.,  
717 Bossi, R., Claeys, M., Dye, C., Evtugina, M., Garc ía-Gacio, D., Hillamo, R., Hoffer, A., Hyder,  
718 M., Iinuma, Y., Jaffrezo, J. L., Kasper-Giebl, A., Kiss, G., Lopez-Mahia, P. L., Pio, C., Piot, C.,  
719 Ramirez-Santa-Cruz, C., Sciare, J., Teinil ä K., Vermeulen, R., Vicente, A., and Zimmermann,  
720 R.: An intercomparison study of analytical methods used for quantification of levoglucosan in  
721 ambient aerosol filter samples, *Atmos. Meas. Tech.*, 8, 125–147, [https://doi.org/10.5194/amt-](https://doi.org/10.5194/amt-8-125-2015)  
722 8-125-2015, 2015.

723 Yuan, Q., Qi, B., Hu, D. Y., Wang, J. J., Zhang, J., Yang, H. Q., Zhang, S. S., Liu, L., Xu, L., and Li,  
724 W. J.: Spatiotemporal variations and reduction of air pollutants during the COVID-19  
725 pandemic in a megacity of Yangtze River Delta in China, *Sci. Total Environ.*, 751, 141820,  
726 <https://doi.org/10.1016/j.scitotenv.2020.141820>, 2021.

727 Zeng, L. H., Dibb, J., Scheuer, E., Katich, J. M., Schwarz, J. P., Bourgeois, I., Peischl, J., Ryerson,  
728 T., Warneke, C., Perring, A. E., Diskin, G. S., DiGangi, J. P., Nowak, J. B., Moore, R. H.,  
729 Wiggins, E. B., Pagonis, D., Guo, H. Y., Campuzano-Jost, P., Jimenez, J. L., Xu, L., and Weber,  
730 R. J.: Characteristics and evolution of brown carbon in western United States wildfires, *Atmos.*  
731 *Chem. Phys.*, 22, 8009–8036, <https://doi.org/10.5194/acp-22-8009-2022>, 2022.

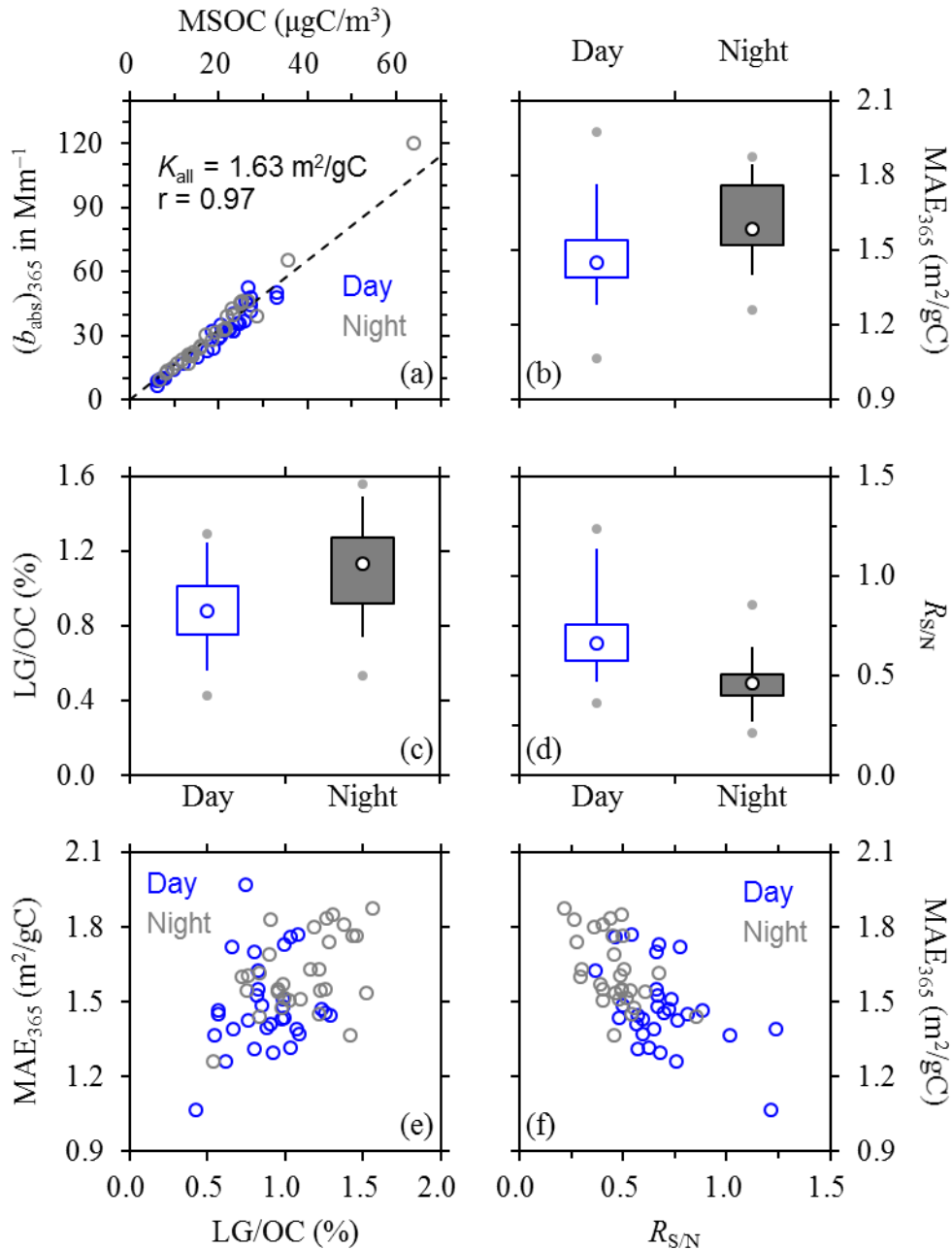
732 Zeng, L. H., Zhang, A. X., Wang, Y. H., Wagner, N. L., Katich, J. M., Schwarz, J. P., Schill, G. P.,  
733 Brock, C., Froyd, K. D., Murphy, D. M., Williamson, C. J., Kupc, A., Scheuer, E., Dibb, J., and  
734 Weber, R. J.: Global measurements of brown carbon and estimated direct radiative effects,  
735 *Geophys. Res. Lett.*, 47, e2020GL088747, <https://doi.org/10.1029/2020GL088747>, 2020.

736 Zeng, Y. L., Ning, Y. L., Shen, Z. X., Zhang, L. M., Zhang, T., Lei, Y. L., Zhang, Q., Li, G. H., Xu,  
737 H. M., Ho, S. S. H., and Cao, J. J.: The roles of N, S, and O in molecular absorption features

738 of brown carbon in PM<sub>2.5</sub> in a typical semi-arid megacity in Northwestern China, *J. Geophys.*  
739 *Res. Atmos.*, 126, e2021JD034791, <https://doi.org/10.1029/2021JD034791>, 2021.

740 Zhang, J., Smith, K. R., Ma, Y., Ye, S., Jiang, F., Qi, W., Liu, P., Khalil, M. A. K., Rasmussen, R.  
741 A., and Thorneloe, S. A.: Greenhouse gases and other airborne pollutants from household  
742 stoves in China: a database for emission factors, *Atmos. Environ.*, 34, 4537–4549,  
743 [https://doi.org/10.1016/S1352-2310\(99\)00450-1](https://doi.org/10.1016/S1352-2310(99)00450-1), 2000.

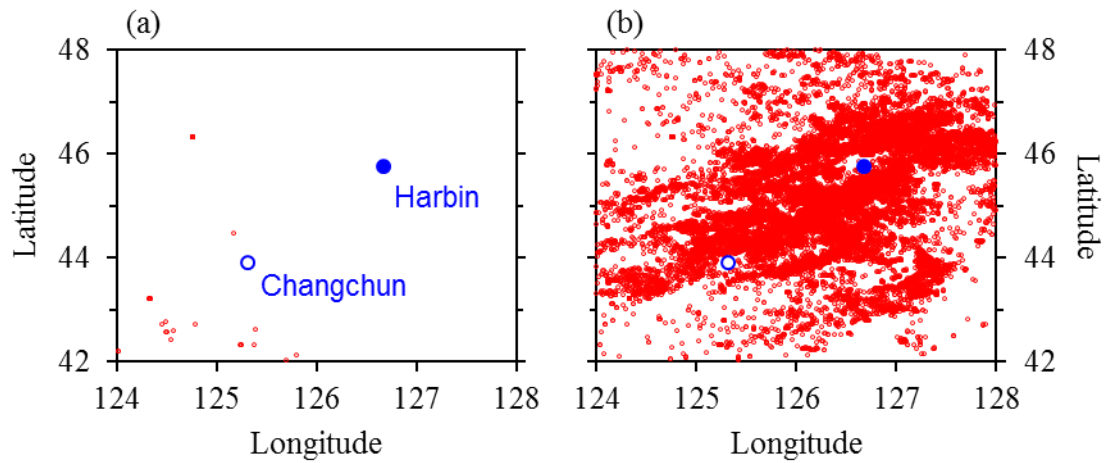
744 Zhang, Y. L., Wang, X. M., Li, G. H., Yang, W. Q., Huang, Z. H., Zhang, Z., Huang, X. Y., Deng,  
745 W., Liu, T. Y., Huang, Z. Z., and Zhang, Z. Y.: Emission factors of fine particles, carbonaceous  
746 aerosols and traces gases from road vehicles: recent tests in an urban tunnel in the Pearl River  
747 Delta, China, *Atmos. Environ.*, 122, 876–884, <https://doi.org/10.1016/j.atmosenv.2015.08.024>,  
748 2015.



749

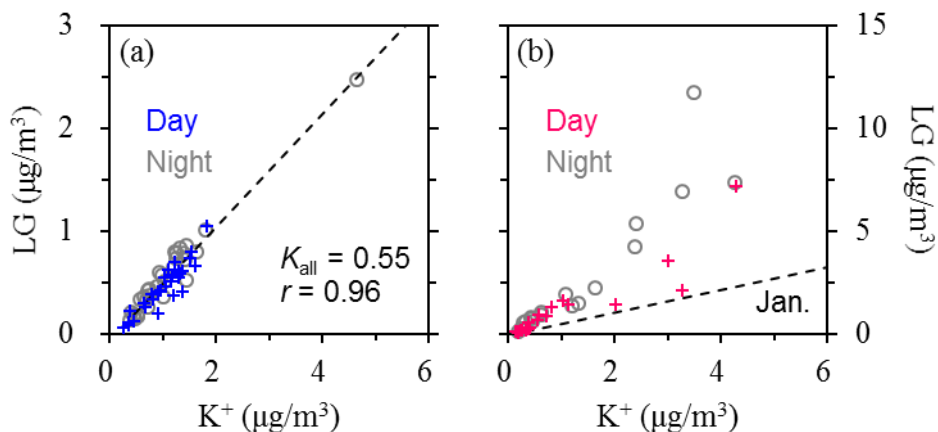
750 **Figure 1.** (a) Dependence of  $(b_{\text{abs}})_{365}$  on MSOC, (b–d) diurnal variations of  $\text{MAE}_{365}$ ,  $\text{LG}/\text{OC}$  (on a  
751 basis of carbon mass) and  $R_{S/N}$ , and (e–f) dependences of  $\text{MAE}_{365}$  on  $\text{LG}/\text{OC}$  or  $R_{S/N}$  during winter.  
752 In (a), the dashed line indicates linear regression result based on all the winter samples, with  $K_{\text{all}}$  as  
753 slope (intercept was set as zero). In (b–d), lower and upper box bounds indicate the 25th and 75th  
754 percentiles, the whiskers below and above the box indicate the 5th and 95th percentiles, the solid  
755 circles below and above the box indicate the minimum and maximum, and the open circle within  
756 the box marks the median (the same hereinafter). Comparison of (e) and (f) suggests that the  
757 wintertime  $\text{MAE}_{365}$  was more strongly influenced by  $R_{S/N}$  compared to  $\text{LG}/\text{OC}$ . The dependence  
758 shown in (f) could be approximated by the following function for all the winter samples ( $r = 0.61$ ):  
759  $\text{MAE}_{365} = (-0.51 \pm 0.09) \times R_{S/N} + (1.84 \pm 0.05)$ .





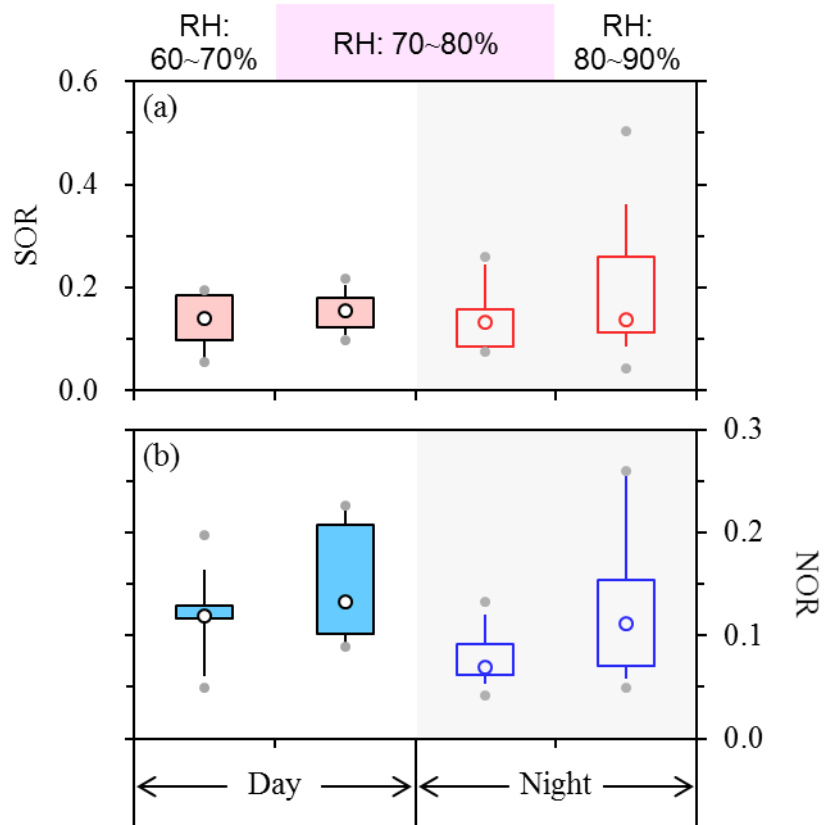
760

761 **Figure 2.** Cumulative fire hotspots detected throughout the (a) winter and (b) spring measurement  
 762 periods around Harbin, with their locations shown by the red circles. The HC metropolitan area has  
 763 two central cities as marked by the blue circles. The fire data were based on the joint NASA/NOAA  
 764 Suomi National Polar-orbiting Partnership (S-NPP) satellite, and were downloaded from the Fire  
 765 Information for Resource Management System (FIRMS; <https://firms.modaps.eosdis.nasa.gov/>, last  
 766 access: 1 January, 2023).



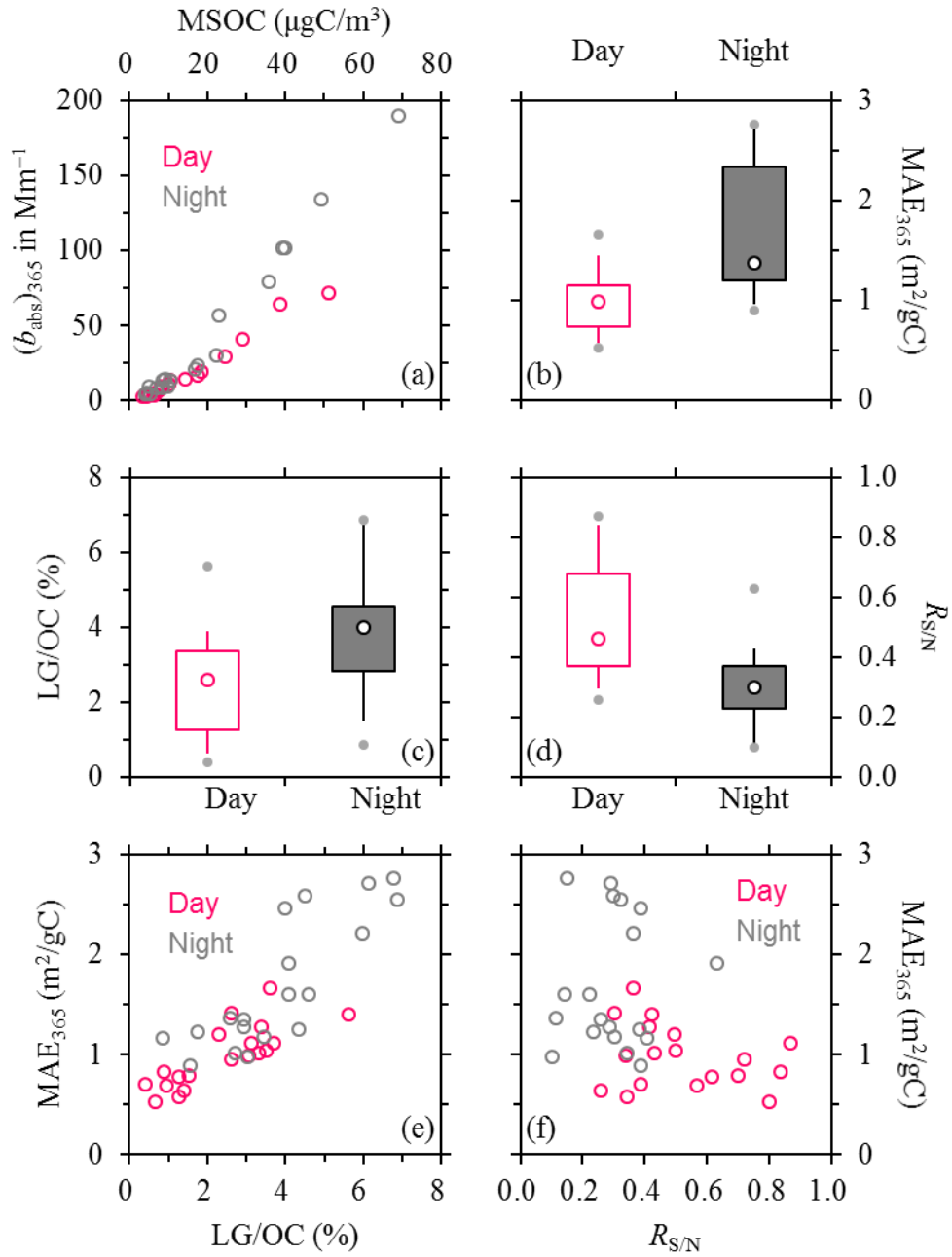
767

768 **Figure 3.** Dependences of levoglucosan on  $K^+$  during (a) winter and (b) spring. In (a), the dashed  
 769 line indicates linear regression result based on all the winter samples, with  $K_{all}$  as slope. The  
 770 regression line of winter campaign is also shown in (b) for comparison to highlight the increased  
 771 and variable  $LG/K^+$  ratios in spring. The relatively low and constant  $LG/K^+$  in winter were attributed  
 772 to residential burning of crop residues, a routine activity occurring every day in rural areas for  
 773 cooking and heating. The higher  $LG/K^+$  in spring were associated with agricultural fires, as  
 774 supported by the intensive fire hotspots detected.



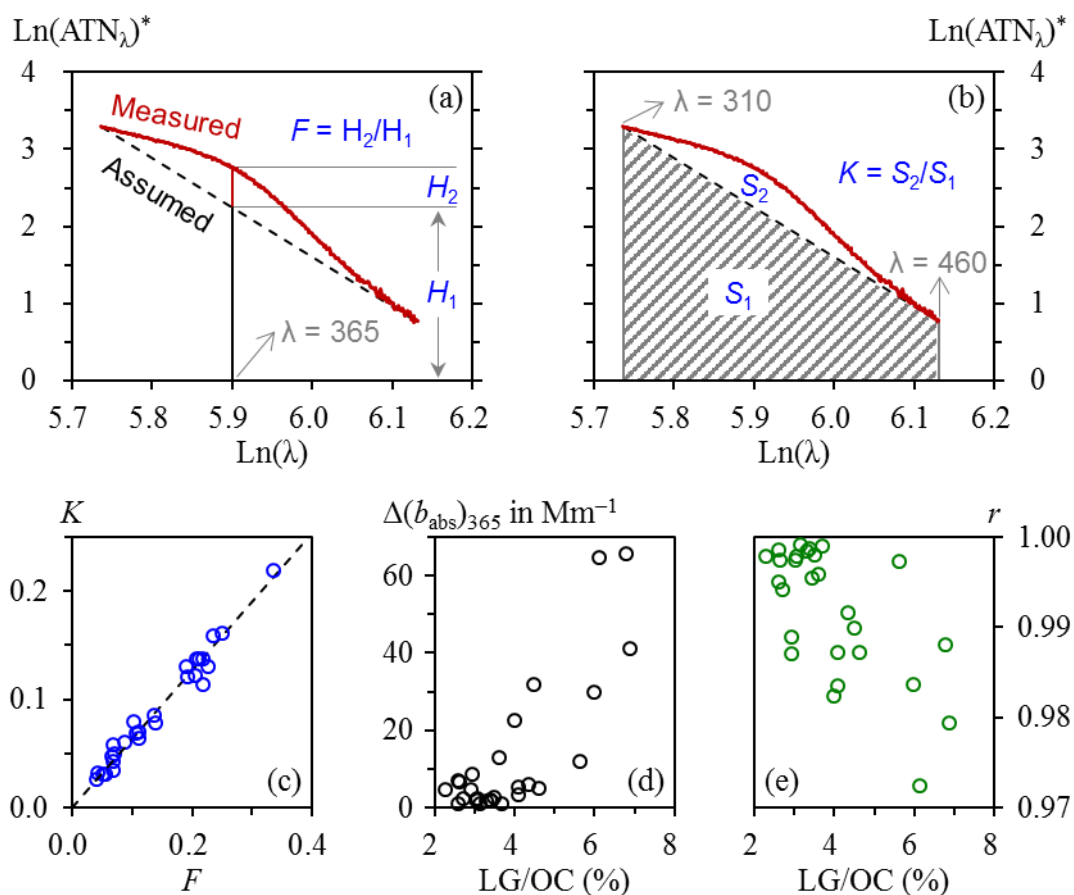
775

776 **Figure 4.** Diurnal variations of (a) SOR and (b) NOR in winter, with results from different RH  
 777 ranges shown separately. Daytime and nighttime samples had a common RH range of 70–80%,  
 778 whereas low RH levels of 60–70% and high RH levels of 80–90% occurred only during the day and  
 779 at night, respectively.



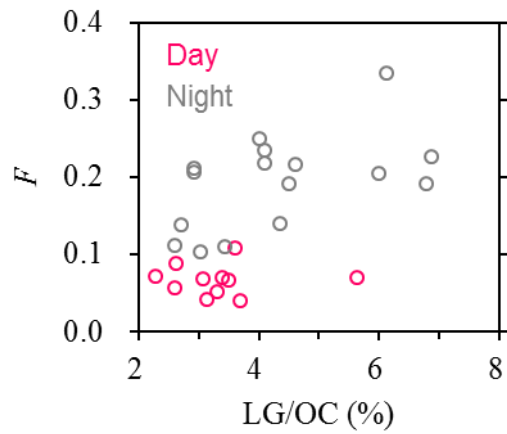
780

781 **Figure 5.** The same as Figure 1 but for spring.  $\text{MAE}_{365}$  showed more pronounced diurnal variations  
 782 in spring than winter, although the daytime vs. nighttime discrepancies in  $R_{\text{S/N}}$  were comparable  
 783 between the two seasons. Comparison of (e) and (f) suggests that unlike winter, the springtime  
 784  $\text{MAE}_{365}$  was more strongly influenced by  $\text{LG}/\text{OC}$  than by  $R_{\text{S/N}}$ . The dependence shown in (e) could  
 785 be approximated by the following function for all the spring samples ( $r = 0.84$ ):  $\text{MAE}_{365} = (30.48 \pm$   
 786  $3.28) \times \text{LG}/\text{OC} + (0.39 \pm 0.12)$ , where  $\text{LG}/\text{OC}$  is on a basis of carbon mass and in %.



787

788 **Figure 6.** Nonlinearity of  $\ln(ATN_\lambda)^*$  on  $\ln(\lambda)$  during agricultural fire episodes in spring: (a–b)  
 789 illustrations of the determination of  $F$  and  $K$ , (c) comparison of  $K$  and  $F$ , and (d–e) dependences of  
 790  $\Delta(b_{\text{abs}})_{365}$  and  $r$  on LG/OC. In (a) and (b), the measured spectrum correspond to the nighttime sample  
 791 collected on April 21, 2021, which had an LG/OC of 6.87%; the assumed spectrum was generated  
 792 by drawing a line between the two points with  $x$  values of  $\ln(310)$  and  $\ln(460)$ ;  $H_1$  indicates  
 793  $\ln(ATN_{365})^*$  of the assumed spectrum, while  $H_2$  indicates the difference in  $\ln(ATN_{365})^*$  between the  
 794 two spectra;  $S_1$  indicates the area enclosed by the assumed spectrum and the  $x$ -axis, while  $S_2$   
 795 indicates the area enclosed between the two spectra. In (c), the dashed line indicates linear regression  
 796 result (intercept was set as zero) and the corresponding  $r$  value was 0.99. In (e),  $r$  was derived from  
 797 linear regression of  $\ln(ATN_\lambda)^*$  on  $\ln(\lambda)$ . Although the  $r$  values seemed reasonable, the AAE results  
 798 should be interpreted with caution given the apparent absorption peak at  $\sim 365$  nm.



799

800 **Figure 7.** Dependence of  $F$ , a measure of the significance of the  $\sim 365$  nm absorption peak, on  
 801 LG/OC during agricultural fire episodes in spring. For a given LG/OC range,  $F$  decreased  
 802 substantially during the day, likely due to photo-bleaching of chromophores associated with the  
 803  $\sim 365$  nm peak. The same conclusion could be reached based on  $K$ , another indicator for the  
 804 significance of the  $\sim 365$  nm peak.